Mechanistic Insights into Benzyne Formation via Di-iodobenzene Photolysis

Cristian Guerra,[*abc] Leandro Ayarde-Henríquez,[*cd] Yeray A. Rodriguez-Nuñez,[c] Eduardo Chamorro[c] and Adolfo E. Ensuncho[b]

[a]Universidad Autónoma de Chile. Facultad de Ingeniería. Avenida Pedro de Valdivia 425, 7500912, Santiago de Chile. Chile.
[b]Universidad de Córdoba. Grupo de Química Computacional. Facultad de Ciencias Básicas. Carrera 6, No.77-305, Montería-Córdoba. Colombia.
[c]Universidad Andrés Bello. Centro de Química Teórica y Computacional (CQT&C). Facultad de Ciencias Exactas. Santiago de Chile. Chile.
[d]Trinity College Dublin, The University of Dublin. School of Physics, College Green Dublin 2, Ireland.

Abstract: We present a comprehensive reaction mechanism for the benzyne formation through the 1,2-diodobenzene photolysis, a topic of major interest in organic synthesis. Our findings firmly support the experiment-based hypothesis of Kharasch and Sharm [*Chem Comm*, **1967**, *10*, 492–493], revealing that C-I bonds break homolytically, and addressing the inherent challenges of this process. Upon photolysis, benzyne and molecular iodine are the ground-state products resulting from a non-adiabatic deactivation, whereas the 2-iodo phenyl radical is produced from the triplet excited state. The confluence of both funnels at the same conical point sharpens the competition, significantly limiting the organic synthesis of aryne. The results indicate that benzyne forms via a two-step process involving the elimination of both iodine atoms.

Introduction

The chemistry of aryl (Ar) halide (X) compounds continues to be an active research field in organic synthesis.[1–9] The reactivity of the Ar-X bond drives a plethora of applications, including cross-coupling synthesis,[10–14] supramolecular chemistry,[15–18] and dehalogenation processes for environmental purposes.[19–21] The pivotal Ar-X bond breaking has a central role within these applications, in which high reactive species such as aryl radicals constitute the crucial component of the overall mechanism.[22–24] It has been shown that the Ar–X bond dissociation is more favorable in electronically excited states due to the notable exergonicity of the Ar-X → Ar + X reaction.[25,26] For iodoaromatic compounds, the photo-production of aryl radicals is challenging because of the coexistence of multiple competing reaction channels within each electronic state, which makes this process inefficient.[27] Indeed, secondary products, such as biphenyls, benzyne derivatives, or even the initial halides (HA), arising from the photo-dissociation reaction, hinder the understanding of the HA mechanism formation and, thus, the synthesis process. In this context, iodobenzenes photochemistry is a particularly appealing field because of the benzyne formation. The experimental studies of Kampmeier and Hoffmeister[28] have provided valuable insights into the dissociation of o-di-iodobenzene, unveiling benzyne's role as an intermediate in Diels-Alder reactions. To the best of our knowledge, two prevailing hypotheses regarding the benzyne formation from o-diodobenzene photolysis have been discussed in the literature:[29,30] (i) the excited o-diodobenzene and (ii) the loss of an iodine atom by 2-iodophenyl radical. Please, see Figure 1.

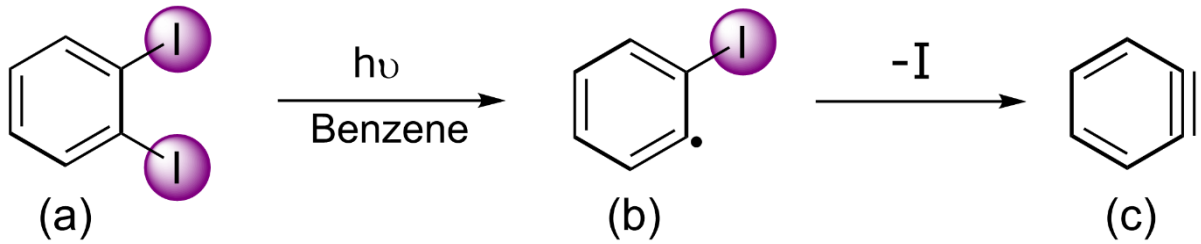

Figure 1. Reaction mechanism of the 1,2-diodobenzene photolysis proposed by Kampmeier and Hoffmeister.[28]

Despite the considerable progress in organic synthesis, the mechanistic intricacies of benzyne formation within HA photochemistry remain relatively unexplored, posing a critical knowledge gap in this field since the existing investigations have failed to provide definitive evidence to resolve this chemical process.[31–36] Experimental studies focusing on o-iodobenzene photolysis, aimed at detecting benzene have yielded inconclusive results, underscoring the need for further exploration. From a theoretical standpoint, identifying the photochemical route leading to benzyne holds profound significance because HA photolysis could be restricted to investigating reactive intermediates of subsequent cycloaddition reactions, unraveling new possibilities for practical applications. In pragmatic terms, elucidating the extent to which the benzyne reaction pathway limits aryl radical synthesis is essential to design efficient strategies and advancing aryl radical synthesis techniques.

Thus, this work aims to address the existing knowledge gap in HA photochemistry by proposing a reaction mechanism for the benzyne generation from iodoaromatic compounds through TD-DFT and ab-initio methods. Our discussion relies on both the exhaustive exploration of the potential energy surface of 1,2-diodobenzene photolysis and the chemical bonding analysis of the electron localization function (ELF) topology.[37–43] Please, see the electronic supplementary information (ESI) for detailed information on the theoretical and computational approaches. Herein, we discussed the mechanistic features of the benzyne formation from o-iodobenzene. However, other similar systems were considered to show the general character and consistency of our findings: o-dichlorobenzene, o-dibromo benzene, 4-methyl o-di-iodobenzene, 4-hydroxy o-di-iodobenzene, 4-cyano o-di-iodobenzene, 4-methoxy o-di-iodobenzene, 4-formyl o-di-iodobenzene, and 4-nitro o-di-iodobenzene. See the ESI for further details.

Results and Discussion

The photolysis of 1,2-diodobenzene is initiated by the $S_0 \rightarrow S_2$ vertical excitation, which is characterized by the C-band in the UV spectrum.[44] Table 1 lists the excitation energies for both $S_0 \rightarrow S_1$ and $S_0 \rightarrow S_2$ transitions at TD-DFT/def2-TZVP and NEVPT2/def2TZVP levels. These excitation energies closely match the experimental data obtained from the UV absorption spectrum of 1,2diodobenzene in hexane, demonstrating the accuracy and consistency of the theoretical predictions.

Table 1 Computed and experimental excitation energies of $S_0 \rightarrow S_1$ and $S_0 \rightarrow S_2$ vertical transitions in the 1,2-diodobenzene photolysis.

Excitation	WB97X	CAM-B3LYP	PBE0	NEVPT2	Exp.
$S_0 \rightarrow S_1$	4.64	4.45	3.78	4.41	4.54
$S_0 \rightarrow S_2$	4.87	4.73	3.98	4.75	5.00

Moreover, the $S_0 \rightarrow S_2$ vertical excitation is mainly characterized by the redistribution of electron density, ρ, over the C1-I1 and C2-I2 bonds. Figure 2 depicts the iso-surface for the electron density difference, $\Delta\rho$, between the S_2 and S_0 states. Red regions indicate electron density depletion, $\Delta\rho < 0$, whereas blue zones represent electron density accumulation, $\Delta\rho > 0$. The high-energy Franck-Condon (FC) structure at S_2 exhibits a notable concentration of electron density over the C1-I1 and C2-I2 bonds, flowing from the I1, I2, C1, and C2 valence shells.

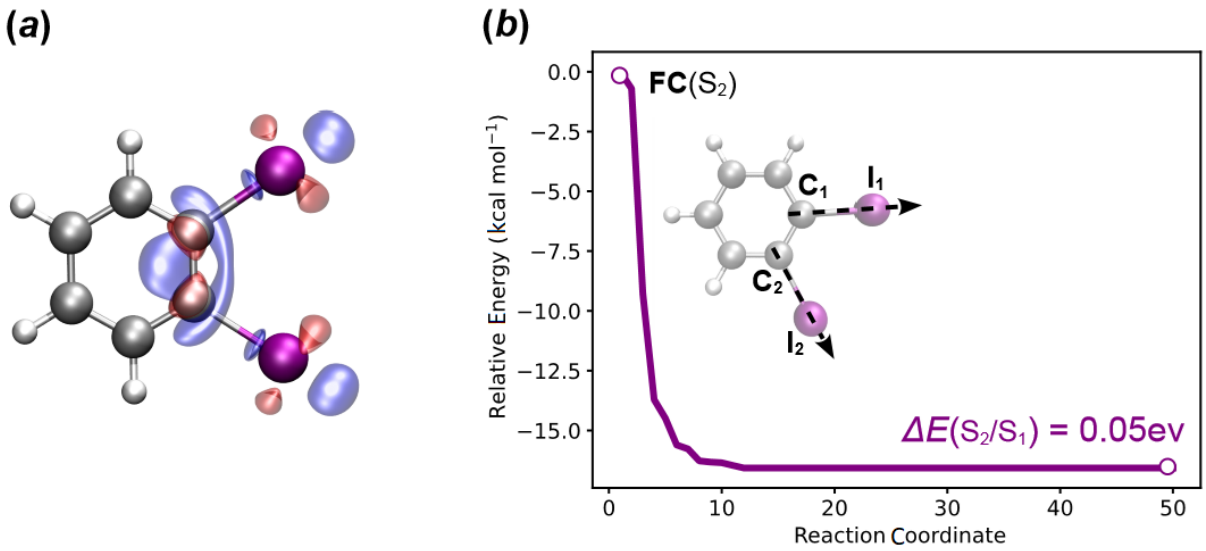

Figure 2. Isosurface of the electron density difference between the S_2 and S_0 states due to $S_0 \rightarrow S_2$, Panel A. Regions in blue indicate electron density concentration, $\Delta\rho > 0$. Red zones represent electron density depletion, $\Delta\rho < 0$. Intrinsic reaction coordinate (IRC) connecting the Franck-Condon (FC) region, S_2, and the first excited state, S_1, Panel B.

At this stage, the stretching of C1-I1 and C2-I2 constitutes the onset of the 1,2-diodobenzene FC-structure deactivation. The system approaches the S_2/S_1 crossing upon further increase of the C2-I2 bond length from 2.09 to 2.43 Å, releasing -17.83 kcal mol^{-1} and facilitating the $S_2 \rightarrow S_1$ transition. It should be noted that this deactivation pathway is also observed in other iodoaromatic compounds; see the ESI for details. Upon departure from the S_2/S_1 crossing, the CI2-I2 bond attains 2.55 Å, signifying the entry into the Min2 radical state (S_1). The minimum energy conical intersection point 2 (MECI-2), S_1/S_0, controls the non-radiative transition along the $S_1 \rightarrow S_0$ process. The C2-I2 bond distance is 2.84 Å, a value considerably higher than the experimental value (1.96-2.00 Å). Concurrently, the separation between the I1 and I2 atoms reduces as the C1-I1 length reaches 2.37 Å. Interestingly, the geometry of MECI-1 suggests that the crossing between S_1 and the ground state induces the C2-I2 bond scission. Within the S_1/S_0 region, the excited 1,2-diodobenzene follows two primary decay channels: MECI-1 → MECI-2 and Min1 → MECI-2. See Figure 3.

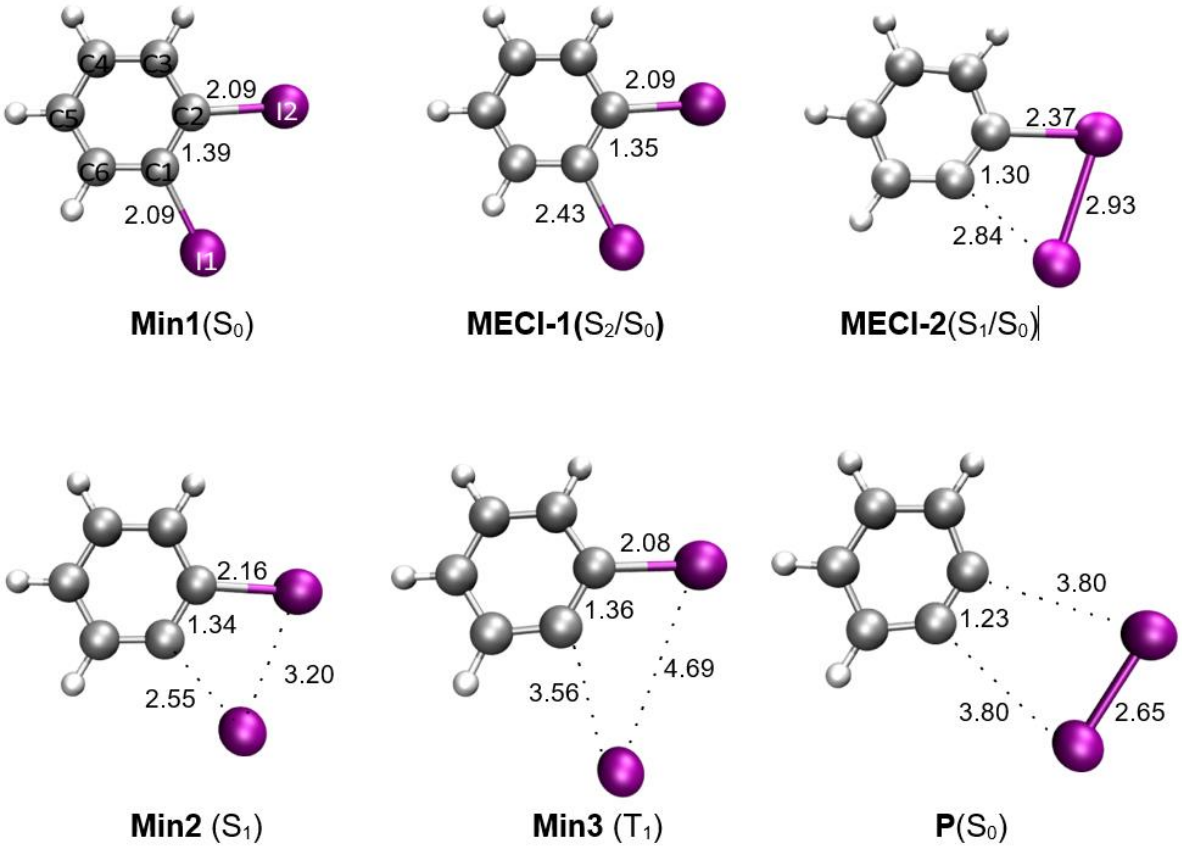

Figure 3. Relevant stationary energy points along the pathway of the 1,2diodobenzene photolysis.

The breaking of the remaining C1-I1 and the I1-I2 forming co-occur as the system departs from the CI, leading to I_2 and benzyne. The formation of the latter is essentially exergonic, liberating -31.47 kcal mol^{-1}. Considering the radical pathway, our results show that the T_1 state nearly degenerates at MECI-1 since the energy gap between S_1 and T_1 ranges from 0.1 to 0.2 eV. Of particular significance is the involvement of Min3 in the benzyne formation through the radical reaction pathway. This process entails the endergonic scission of the C1-I1 bond, as shown in Figure 4.

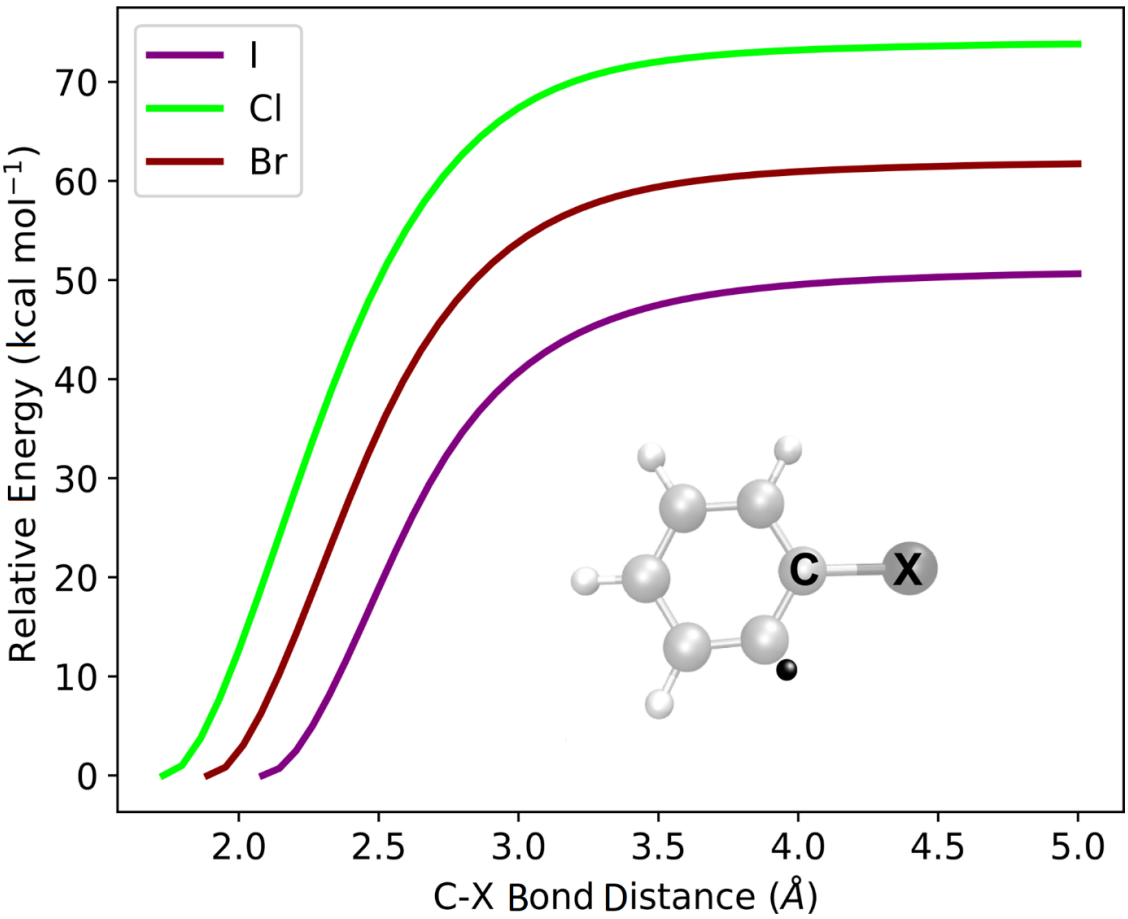

Figure 4. Dissociation energy of ArX$^{\bullet}$ → benzyne + X$^{\bullet}$ processes, where X=Cl, Br, I.

Notably, the computed C-I dissociation energy in the context of 1,2-diodobenzene photolysis is about 50 kcal mol^{-1}, indicating a substantial energy demand for benzyne generation through the 2-iodophenyl radical pathway. Consequently, Min3 is more likely involved in biphenyl formation than benzyne production. In contrast, the non-radical path (MECI-2) plays a crucial role in the benzyne production mechanism. Figure 5 depicts the IRC of MECI-2 → Min3 and MECI-2 → P processes. The benzyne species present at MECI-2 can form via the non-adiabatic deactivation $S_1 \rightarrow S_0$. It is worth noting that the benzyne production from Min3 is unlikely to occur even though a reaction pathway connects MECI-2 and Min3. In general, the non-radical mechanism for the benzyne formation involves two crucial reaction stages: (i) the fast traversal through the S_2/S_1 crossing and (ii) the fast transition toward ground or T_1 states, yielding benzyne. The first reaction stage comprises the C1-I1 bond weakening near the MECI-1 point. Subsequently, the cleavage of C2-I2 initiates at S_1, and the I—I interaction strengthens upon further evolution of the reaction system towards the MECI-2 configuration. If the system reaches T_1, the C1-I1 bond will finally break forming the 2-iodo-phenyl radical. The cleavage of the remaining C2-I2 bond yields benzyne and molecular iodine.

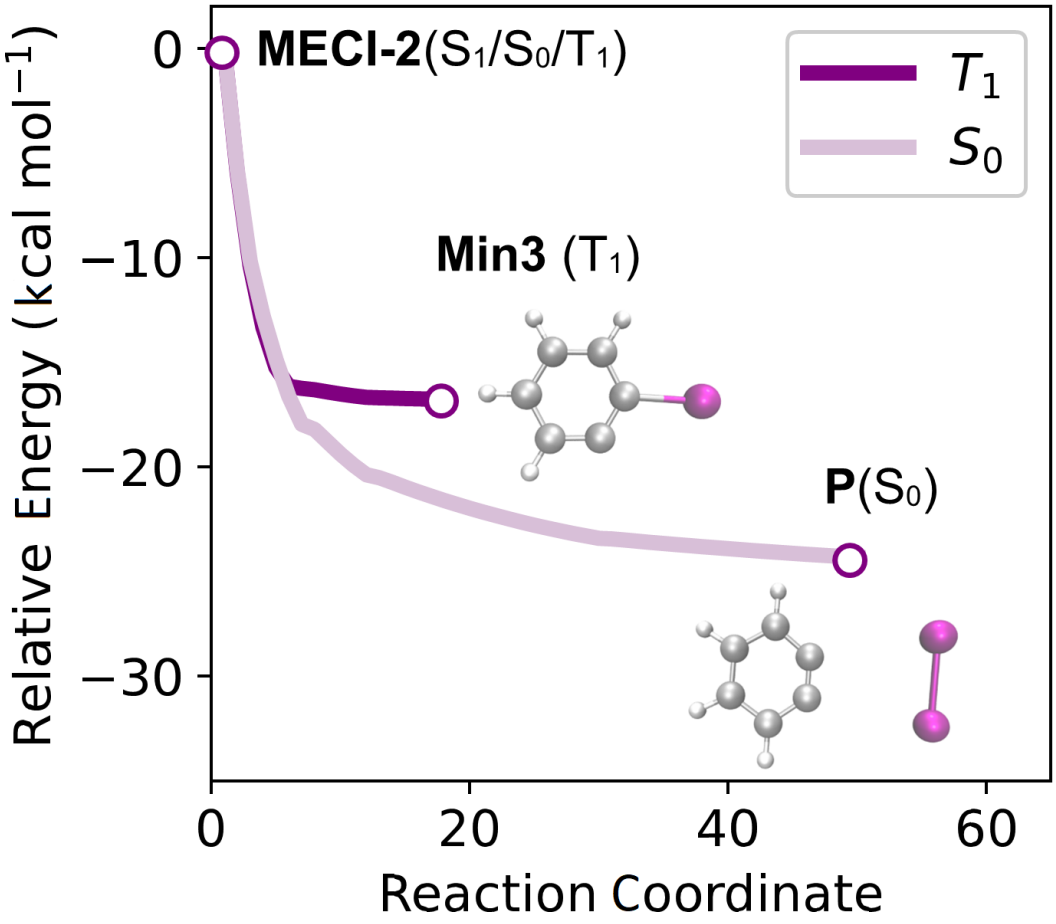

Figure 5. IRC of the benzyne and 2-iodo phenyl radical productions from MECI-2. Benzyne forms at S_0, while the radical upon deactivation from T_1.

Our results reveal the feasibility of both radical and nonradical mechanisms originally proposed by Kharasch and Sharm, involving non-adiabatic transitions mediated by MECI-2 and MECI-1. The energetic barrier associated with the MECI-1 → MECI-2 process is relatively low, 8.48 kcal mol^{-1}, which suggests that the S_1/S_0 funnel is reasonably accessible from the S_2 surface. This trend is also observed in functionalized 1,2-diodobenzenes, as shown in Table 2.

Table 2 Formation enthalpies at 0 K, ΔH, of the MECI-1 → MECI-2, MECI-2 → Min3, and MECI-2 → P processes in substituted 1,2,4-diiodobenzenes.

System	MECI-1 → MECI-2	MECI-2 → Min3	MECI-2 → P
CH_3	9.95	-48.53	-38.50
CHO	-7.18	-44.37	-29.14
CN	4.23	-37.48	-28.71
NO_2	8.69	-24.51	-29.45
OCH_3	-0.14	-26.34	-12.14
OH	-0.09	-26.02	-28.35

Outcomes derived from the electron rearrangements analysis applied to the 1,2-diodobenzene photolysis is a valuable complementary approach for the energy-based mechanistic discussion, offering in-depth insights into the

underlying density fluxes governing the reaction.[45–49] Considering that ELF provides a direct connection with Lewis objects, such as core, lone pares, bonds, and valence,[50–54] we analyzed the topography of this function at each stationary point. Note that the V(A) (monosynaptic) basin represents the non-bonding electrons of the A atom, whereas the V(A,B) (disynaptic) basin indicates the electron density shared by the A and B atoms. Table 3 lists the electron population of ELF basins at the most relevant stationary points.

Table 3 Electronic populations, e, of monosynaptic and disynaptic basins at stationary points featuring the 1,2-diodobenzene photolysis.

Basin	MECI-1	MECI-2	P	Min3	Min1
V(C1,C2)	2.73	3.17	3.42	2.84	2.87
V(C2,I2)	1.64	1.54	-	1.68	1.78
V(C1,I1)	1.32	-	-	-	1.78
V(I1,I2)	-	-	1.20	-	-
V(C1)	-	0.88	0.80	1.09	-
V(C2)	-	-	0.80	-	-
V(I1)	7.29	7.32	6.61	7.25	6.45
V(I2)	6.62	6.53	6.61	6.57	6.45

The assessment of ELF basins confirms the previously observed C1-I1 bond weakening, showing that the population of this bond decreases by 0.46e. This amount mainly accumulates over the non-shared valence shell of I1. Figure 6 presents some ELF contour plots which further support the current discussion.

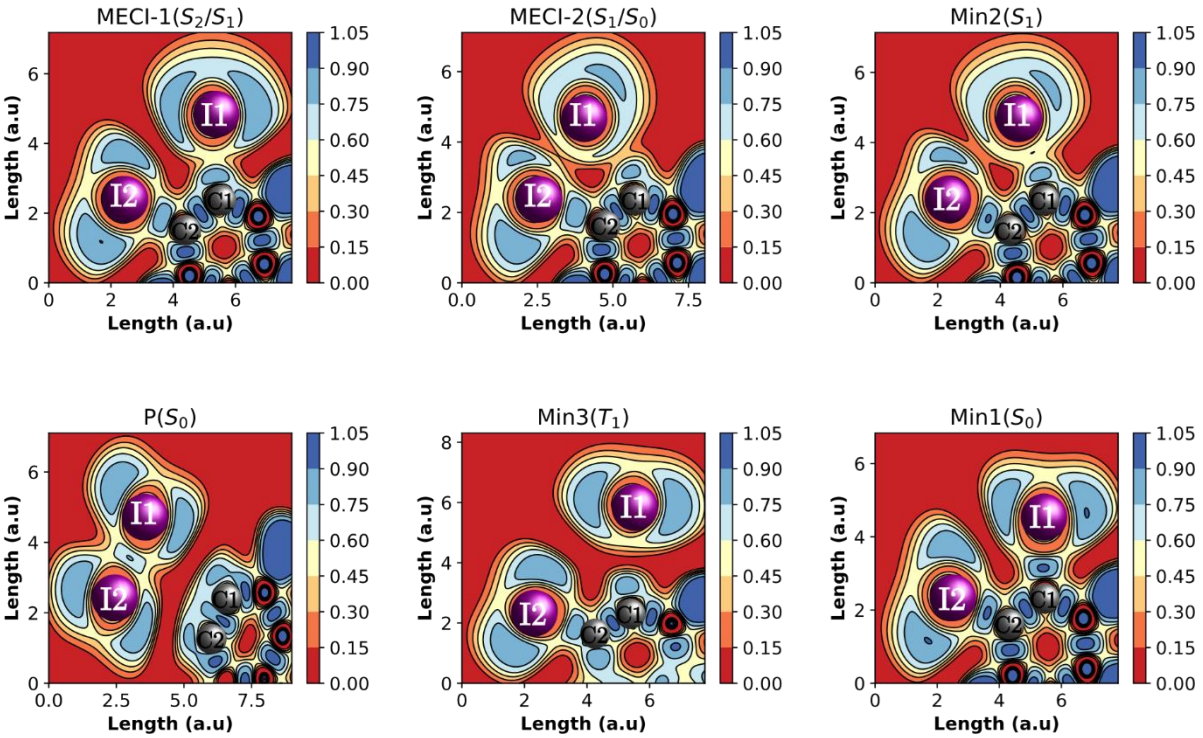

Figure 6. ELF contour plots of relevant stationary points in the 1,2-di-iodobenzene photolysis. ELF is plotted for the plane formed by the I1, C1, C2, and I2 atoms. The isosurface value is 0.89.

Furthermore, the Min1 → MECI-1 process comprises the splitting of the pairing density shared by C1 and I1. Thus, the C1-I1 bond weakening (at S_2) implies the migration of electron density towards I1. This is evident from the increase in the ELF value near this atom. Then, the C1-I1 finally breaks along the MECI-1 → MECI-2 deactivation, resulting in the formation of a radicaloid center (0.88e) near C1, suggesting this bond breaks homolytically. As a result, the electron pairing density flows from V(C1,I1) towards V(C1,C2), increasing its population to 3.17e. A visual inspection of MECI-2 (see Figure 6) confirms that, at this point, the interaction between I1 and I2 valence shells is strong enough, and both regions overlap. Nonetheless, the V(C2,I2) population does not vary significantly; therefore, this bond is unlikely to break at the S_1 state. Once the system departs from S_1/S_0, and approaches the ground state, C2-I2 cleavages through a similar pattern, i.e., yielding a radicaloid center (0.80e) near C2. Moreover, V(I1,I2) forms, integrating 1.2e and the V(C1,C2) population increases up to 3.41e, which indicates the initial stage of a triple bond. Finally, the splitting between I and C atoms' valence shells evidence the formation of both benzyne and molecular iodine products; see Figure 6, Panel P(S_0).

Both C1-I1 and C2-I2 cleavages are crucial in the 1,2-diodobenzene photolysis. These elementary bonding processes result in the formation of radicaloid centers at both C1 and C2 atoms. The appearance of diradical species is a frequent event featuring excited-state reactions.[55–57]Specifically, the radicaloid structures appear along the MECI-2 → P and MECI-2 → Min3 processes. For the ground state route, the density coupling of C1 and C2 radicaloid centers resulting from the C-I scissions leads to the C1-C2 triple bond formation.[58,59] Indeed, the ELF contour plot shows a localization region over C1 and C2; see Figure 6, Panel P(S_0). In contrast, the triplet pathway triggers a radical behavior of 2-iodo phenyl since non-shared density appears over C1 only; see Figure 6, Panel Min3(T_1).

In light of the current discussion, our findings give major support to the hypothesis of Kharasch and Sharm, which states that benzene formation occurs during an initial stage upon the excitation of 1,2-diodobenzene. This stage is characterized by two successive non-adiabatic transitions, comprising the second singlet and the ground states. The first transition induces the cleavage of one C-I bond and facilitates the I-I interaction. The second one predominantly involves the scission of the remaining C-I bond and the formation of both the I-I single and C-C triple bonds. Furthermore, our findings suggest that the C-I bonds, even within the excited states, break homolytically, as depicted in Figure 7.

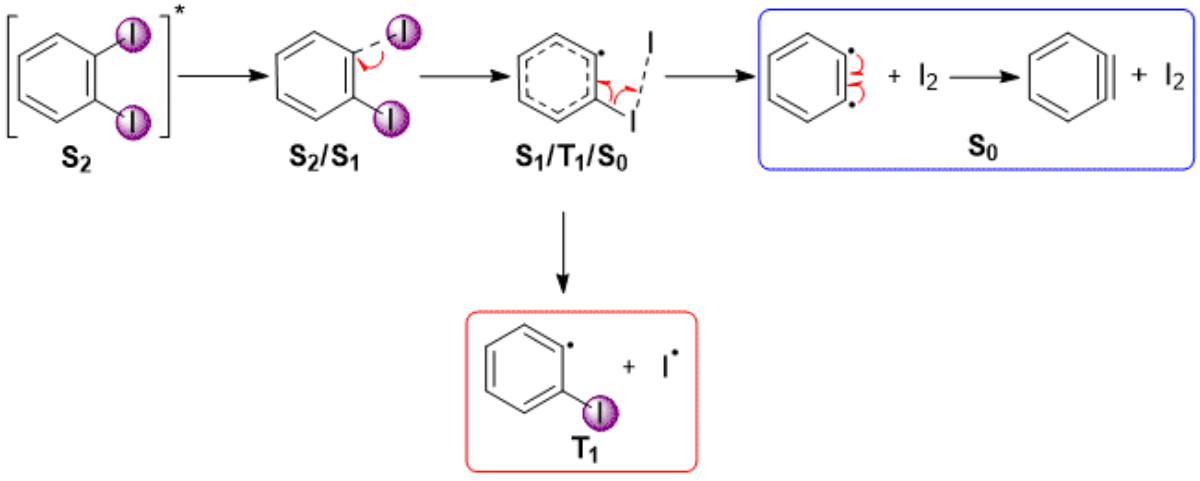

Figure 7. Proposed reaction mechanism for the benzyne and 2-iodophenyl radical formations.

Concluding Remarks

In summary, we have proposed a well-supported reaction mechanism, elucidating the benzyne and 2-iodophenyl radical formations through the 1,2-diodobenzene photolysis. Our findings validate Kharasch and Sharm's hypothesis based on experimental observations. We also tested a series of functionalized 1,2-diodobenzene, with a specific focus on 2-iodobenzene since it exhibits the intriguing feature of generating radicals and benzene byproduct. These findings deepen our understanding of the intricate photochemistry of halogenated aromatic systems, offering a rational and accessible framework for benzyne production. We hope these insights motivate experimental investigations to validate the proposed reaction mechanism, fostering novel methodologies for efficient arynes synthesis.

Computational Methodology

Geometry optimization and vibrational frequencies were carried out using the ORCA 4.2.1 program[60] at the TD-DFT/def2-TZVP level in combination with the wB97X, CAM-B3LYP, and PBE0 global hybrid functionals for 1,2-diodobenzene species. The polarizable continuum model (CPCM) with the benzene solvent was used in all geometry calculations. The intrinsic reaction coordinate (IRC) was computed to find paths connecting the minimum energy conical intersection points (MECIs),[61] determined by the gradient projection method regarding the non-adiabatic couplings, and the ground state. The correlated version of ELF[41,62] was computed (via the first-order density matrix derived from CASSCF calculations available in Multiwfn[63]) for performing the chemical bonding analysis. An active space of 14 electrons distributed over 10 orbitals was considered to calculate the correlated wave function of each stationary point. The dynamic correlation was included through the NEVPT2 approach.

Conflicts of interest

There are no conflicts to declare.

Notes and references

1 R. L. Sutar and S. M. Huber, *ACS Catalysis*, 2019, **9**, 9622–9639.
2 F. Bellina, *Synthesis*, 2021, **53**, 2517–2544.
3 D. Petzold, M. Giedyk, A. Chatterjee and B. König, *European Journal of Organic Chemistry*, 2020, **2020**, 1193–1244.
4 R. Matsubara, T. Yabuta, U. Md Idros, M. Hayashi, F. Ema, Y. Kobori and K. Sakata, *Journal of Organic Chemistry*, 2018, **83**, 9381–9390.
5 O. Sadek, M. Abdellaoui, A. Millanvois, C. Ollivier and L. Fensterbank, *Photochemical and Photobiological Sciences*, 2022, **21**, 585–606.
6 S. Song, X. Li, J. Wei, W. Wang, Y. Zhang, L. Ai, Y. Zhu, X. Shi, X. Zhang and N. Jiao, *Nature Catalysis*, 2020, **3**, 107–115.
7 Y. Wang, Z. Cao, Q. He, X. Huang, J. Liu, H. Neumann, G. Chen and M. Beller, *Chemical Science*, 2023, **14**, 1732–1741.
8 T. Uchikura, K. Tsubono, Y. Hara and T. Akiyama, *Journal of Organic Chemistry*, 2022, **87**, 15499–15510.
9 T. Constantin, M. Zanini, A. Regni, N. S. Sheikh, F. Juliá and D. Leonori, *Science*, 2020, **367**, 1021–1026.
10 H. Hayashi, B. Wang, X. Wu, S. J. Teo, A. Kaga, K. Watanabe, R. Takita, E. K. Yeow and S. Chiba, *Advanced Synthesis and Catalysis*, 2020, **362**, 2223–2231.
11 G. Albano, A. Punzi, M. A. M. Capozzi and G. M. Farinola, *Green Chemistry*, 2022, **24**, 1809–1894.
12 Y. M. Tian, E. Hofmann, W. Silva, X. Pu, D. Touraud, R. M. Gschwind, W. Kunz and B. König, *Angewandte Chemie - International Edition*, 2023, **202218775**, 1–12.
13 V. Palani, M. A. Perea and R. Sarpong, *Chemical Reviews*, 2022, **122**, 10126– 10169.
14 Y. Zhao and W. Xia, *Organic and Biomolecular Chemistry*, 2019, **17**, 4951–4963.
15 J. C. Christopherson, F. Topi´c, C. J. Barrett and T. Friš˘ci´c, *Crystal Growth and Design*, 2018, **18**, 1245–1259.
16 C. Gropp, B. L. Quigley and F. Diederich, *Journal of the American Chemical Society*, 2018, **140**, 2705–2717.
17 F. Eisenreich, T. H. Kuster, D. van Krimpen and A. R. Palmans, *Molecules*, 2021, **26**, 0–11.
18 M. Saccone, M. Spengler, M. Pfletscher, K. Kuntze, M. Virkki, C. Wölper, R. Gehrke, G. Jansen, P. Metrangolo, A. Priimagi and M. Giese, *Chemistry of Materials*, 2019, **31**, 462–470.
19 G. Qiu, Y. Li and J. Wu, *Organic Chemistry Frontiers*, 2016, **3**, 1011–1027.
20 A. Elhage, P. Costa, A. Nasim, A. E. Lanterna and J. C. Scaiano, *Journal of Physical Chemistry A*, 2019, **123**, 10224–10229.
21 D. Cao, C. Yan, P. Zhou, H. Zeng and C. J. Li, *Chemical Communications*, 2019, **55**, 767–770.
22 N. Kvasovs and V. Gevorgyan, *Chem. Soc. Rev.*, 2021, **50**, 2244–2259.
23 F. Yu, R. Mao, M. Yu, X. Gu and Y. Wang, *The Journal of Organic Chemistry*, 2019, **84**, 9946–9956.
24 I. Ghosh, T. Ghosh, J. I. Bardagi and B. König, *Science*, 2014, **346**, 725–728.
25 R. S. Davidson, J. W. Goodin and G. Kemp, *G. Kemp*, Academic Press, 1984, vol. 20, pp. 191–233.
26 J. Grimshaw and A. P. de Silva, *Chem. Soc. Rev.*, 1981, **10**, 181–203.
27 W. Wolf and N. Kharasch, *The Journal of Organic Chemistry*, 1965, **30**, 2493– 2498.
28 J. A. Kampmeier and E. Hoffmeister, *Journal of the American Chemical Society*, 1962, **84**, 3787–3788.
29 N. Kharasch and R. K. Sharma, *Chemical Communications*, 1967, 492–493.
30 C. Ogat, W. Wolf and N. Kharasch, *The Journal of Organic Chemistry*, 1965, **1843**, 2493–2498.
31 S. Protti, V. Dichiarante, D. Dondi, M. Fagnoni and A. Albini, *Chemical Science*, 2012, **3**, 1330–1337.

32 M. Chen, C. He, X. Bai, D. Zhao and Y. Chen, *Journal of Chemical Physics*, 2017, **147**, 29–31.
33 A. G. Sage, T. A. Oliver, D. Murdock, M. B. Crow, G. A. Ritchie, J. N. Harvey and M. N. Ashfold, *Physical Chemistry Chemical Physics*, 2011, **13**, 8075–8093.
34 H. H. Wenk and W. Sander, *Eur. J. Org. Chem*, 2002, 3927–3935.
35 R. E. F. , Hillinski; P. M., *J. Am. Chem. Soc*, 1985, **107**, 5907–5910.
36 M. Protocol, C. Cao, Y.-w. Chen, Y. Wu and E. Deumens, *International Journal of Quantum Chemistry*, 2009, **109**, 1962–1974.
37 A. Savin, B. Silvi and F. Colonna, *Canadian Journal of Chemistry*, 1996, **74**, 1088–1096.
38 A. Savin, R. Nesper, S. Wengert and T. F. Fässler, *Angewandte Chemie International Edition in English*, 1997, **36**, 1808–1832.
39 J. Andrés, P. González-Navarrete and V. S. Safont, *International Journal of Quantum Chemistry*, 2014, **114**, 1239–1252.
40 J. Andrés, S. Berski and B. Silvi, *Chemical Communications*, 2016, **52**, 8183– 8195.
41 E. Matito, B. Silvi, M. Duran and M. Solà, *The Journal of Chemical Physics*, 2006, **125**, 024301.
42 B. Silvi and A. Savin, *Nature*, 1994, **371**, 683–686.
43 A. D. Becke and K. E. Edgecombe, *The Journal of Chemical Physics*, 1990, **92**, 5397–5403.
44 J. C. Dearden and W. F. Forbes, *Canadian Journal of Chemistry*, 1955, **37**, 1145– 1154.
45 L. Ayarde-Henríquez, C. Guerra, M. Duque-Noreña, E. Rincón, P. Pérez and E. Chamorro, *J Phys Chem A*, 2021, **125**, 5152–5165.
46 L. Ayarde-Henríquez, C. Guerra, M. Duque-Noreña, E. Rincón, P. Pérez and E. Chamorro, *Chem Phys Chem*, 2022, **23**, e202200343.
47 E. Chamorro, C. Guerra, L. Ayarde-Henríquez, M. Noreña-Duque P. Pérez and E. Rincón, in Chemical Reactivity: Theories and Principles, eds. S. Kayas, L. von Szentpály, G. Serdaroglu and L. Guo, Elsevier, 2023, vol. 1, pp. 465–481.
48 L. Ayarde-Henríquez, C. Guerra, M. Duque-Noreña and E. Chamorro, *Phys Chem Chem Phys*, 2023, **25**, 14274–14284.
49 L. Ayarde-Henríquez, C. Guerra, M. Duque-Noreña and E. Chamorro, *New J Chem*, 2022, **46**, 12002–12009.
50 C. Guerra, L. Ayarde-Henríquez, M. Duque-Noreña, C. Cárdenas, P. Pérez and E. Chamorro, *Phys Chem Chem Phys*, 2021, **23,** 20598–20606.
51 C. Guerra, L. Ayarde-Henríquez, M. Duque-Noreña and E. Chamorro, *J Phys Chem A*, 2022, **126**, 395–405.
52 C. Guerra, L. Ayarde-Henríquez, M. Duque-Noreña and E. Chamorro, *Chem Phys Chem*, 2022, **23**, 202200217.
53 C. Guerra, L. Ayarde-Henríquez, Y. A. Rodríguez-Núñez, A. Ensuncho and E. Chamorro, *Chem Phys Chem*, 2023, **24**, e202200867.
54 C. Guerra, L. Ayarde-Henríquez, M. Duque-Noreña and E. Chamorro, *Chem Phys Chem*, 2021, **22**, 2342–2351
55 L. R. Domingo, *RSC Advances*, 2014, **4**, 32415–32428.
56 J. Michl and V. Bona˘ci´c-Koutecký, *Tetrahedron*, 1988, **44**, 7559–7585.
57 C. Guerra, L. Ayarde-Henríquez, E. Chamorro and A. Ensuncho, *ChemPhotoChem*, 2023, **7**, e202200263.
58 E. Kraka and D. Cremer, *Journal of the American Chemical Society*, 1994, **116**, 4929–4936.
59 D. G. Leopold, A. E. S. Miller and W. C. Lineberger, *Journal of the American Chemical Society*, 1986, **108**, 1379–1384.
60 F. Neese, *WIREs Computational Molecular Science*, 2012, **2**, 73–78.
61 I. J. Palmer, I. N. Ragazos, M. A. Robb, F. Bernardi and M. Olivucci, *Journal of the American Chemical Society*, 1993, **115**, 673–682.
62 F. Feixas, E. Matito, M. Duran, M. Solà and B. Silvi, *Journal of Chemical Theory and Computation*, 2010, **6**, 2736–2742.
63 T. Lu and F. Chen, *Journal of Computational Chemistry*, 2012, **33**, 580–592.